DOI:
10.1016/j.bbamem.2015.11.007

Document Version
Peer reviewed version

The Influence of Rough Lipopolysaccharide Structure on Molecular Interactions with Mammalian Antimicrobial Peptides.

Gianluca Bello,[†,‡] Alice Bodin,[¶] M. Jayne Lawrence,[†] David Barlow,[†] A. James Mason,[†] Robert D. Barker,[*,§] and Richard D. Harvey[*,†]

[†]*Institute of Pharmaceutical Science, King's College London, 150 Stamford Street, London SE1 9NH, U.K.*

[‡]*Department of Nanobiotechnology, University of Natural Resources and Life Science, Muthgasse 11/II, Vienna 1190, Austria*

[¶]*Laboratoire Réactions et Génie des Procédés, UMR-7274, plateforme SVS, 13 rue du bois de la Champelle, 54500 Vandœuvre-lés-Nancy, France*

[§]*Institut Laue-Langevin, 71 avenue des Martyrs, 38042 Grenoble, France*

E-mail: barker@ill.eu; richard.d.harvey@kcl.ac.uk

Abstract

The influence of *E. coli* rough lipopolysaccharide chemotype on the membrane activity of the mammalian antimicrobial peptides (AMPs) human cathelicidin (LL37) and bovine lactoferricin (LFb) was studied on bilayers using solid state ^{2}H NMR (ssNMR) and on monolayers using the subphase injection technique, Brewster angle microscopy (BAM) and neutron reflectivity (NR). The two AMPs were selected because of their differing biological activities. Chain-deuterated dipalmitoylphosphatidylcholine (d_{62}-DPPC) was added to the LPS samples, to highlight alterations in the system

properties caused by the presence of the different LPS chemotypes and upon AMP challenge. Both LPS chemotypes showed a temperature dependent influence on the packing of the DPPC molecules, with a fluidizing effect exerted below the DPPC phase transition temperature (T_m), and an ordering effect observed above the T_m. The magnitude of these effects was influenced by LPS structure; the shorter Rc LPS promoted more ordered lipid packing compared to the longer Ra LPS. These differential ordering effects in turn influenced the penetrative activity of the two peptides, as the perturbation induced by both AMPs to Ra LPS-containing models was greater than that observed in those containing Rc LPS. The NR data suggests that in addition to penetrating into the monolayers, both LL37 and LFb formed a non-interacting layer below the LPS/DPPC monolayer. The overall activity of LL37, which showed a deeper penetration into the model membranes, was more marked than that of LFb, which appeared to localise at the interfacial region, thus providing evidence for the molecular origins of their different biological activities.

1 Introduction.

The external leaflet of the outer membrane (OM) of Gram-negative bacteria is mainly composed of the essential, negatively charged, macroamphiphile lipopolysaccharide (LPS). In bacteria under physiological conditions, OM LPS is cross-linked with Mg^{2+} ions and acts as first line of defence against environmental perturbations, competing microorganisms and in the case of symbiotic bacteria, against the hosts immune system.[1–4] The protective role of the OM affects also the microbicidal activity of drugs used in the treatment of bacterial infections[3,5] leading to a reduced susceptibility of Gram-negative bacteria to common antiseptics and antibiotics compared with Gram-positives.[6,7] By virtue of their ability to effectively breach the barrier of the OM, particular attention has been paid to antimicrobial peptides (AMPs) as possible therapeutics or adjuvant treatments for highly resistant microbial infections.[8,9] Different Gram-negative bacterial strains may express structurally diverse LPS chemotypes (Figure 1) with distinct physico-chemical properties which impart different characteristics to

the OM.[10] Mutant strains expressing truncated, so-called Rough LPS chemotypes are more susceptible to antibiotics, when compared to the wild-type, and, because of this enhanced vulnerability they are considered to be suitable for peptide-membrane interaction studies designed to elucidate the mechanism of action of AMPs on the OM.[4,11] The membrane disrupting activity of AMPs depends on the active conformation adopted by the peptides as well as the composition of the membrane.[12] To date however, AMP-membrane interaction studies have largely ignored the effect of LPS on membrane models.[13–16]

In this study we have investigated the influence of both peptide conformation and LPS chemotype on their molecular interactions, using the α-helical human peptide cathelicidin (LL37) and the β-sheet-forming bovine lactoferricin peptide (LFb) together with two LPS chemotypes from *E. coli* rough mutants. The range of MIC values for for LL37[17,18] and LFb[19–21] can vary largely across literature depending on the *E. coli* strain and the test conditions used. The reported MIC values for LL37 and LFb against th smooth *E. coli* ATCC 25922 are respectively $\sim$0.6 μM[22] and 10 μM,[23] suggesting that LL37 is $\sim$16 times more active than LFb. With regard to their mechanisms of action, both peptides have been shown to interact with, perturb and eventually permeabilize both natural bacterial membranes and synthetic lipid membranes.[20,24–29] LPS has been shown to be a determinant for LL37 and LFb binding and activity,[30–34] making an investigation into their molecular interactions with the OM a key step in understanding their different efficacies against *E. coli* (and possibly other Gram negatives). The realisation of such an investigation necessitates the use of suitable OM mimetics which will remain stable over the timescales needed to conduct biophysical experiments. For example, LPS has been successfully incorporated into planar artificial membrane mimetics stabilised with dipalmitoylphosphatidylcholine (DPPC), for use in neutron reflectivity studies.[35] For the interaction studies presented here, the OM mimetics used were monolayers and multilamellar liposomes composed of mixtures of *E. coli* EH100 Ra LPS or *E. coli* J5 Rc LPS (Figure 1), together with chain-deuterated and fully hydrogenated DPPC. The DPPC provides a platform into which to anchor the LPS chains without imposing any additional packing constraints on planar membrane mimetics, due

to its cylindrical molecular shape. The zwitterionic nature of DPPC reduces the likelihood of any direct electrostatic interaction with AMPs , allowing us to focus on the interactions promoted by the LPS alone.

The order parameters of the fatty acyl moieties of the chain-deuterated d_{62}-DPPC within multilamellar liposomes were used in this study to examine the influence of LPS on bilayer order in solid state ^{2}H NMR (ssNMR) experiments.[36] Liposomes containing mixtures of h-DPPC and d_{62}-DPPC with either J5 Rc LPS or EH100 Ra LPS were analysed by ssNMR in order to examine the effects of the two LPS chemotypes on bilayer packing, thus aiding the understanding of the structural role of LPS in the OM of bacteria. The same technique was also used to study the effect of the interaction of the two AMPs on the DPPC acyl chain order parameters of the liposomes in the presence of 20 mol% LPS.[37]

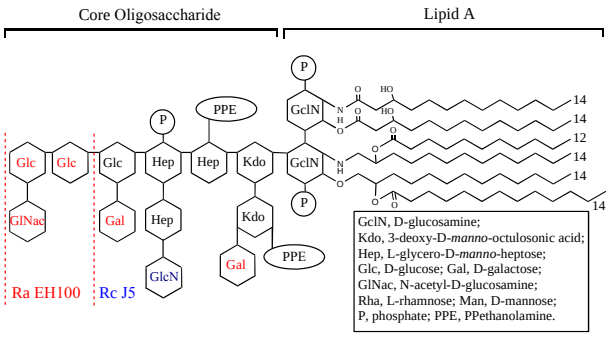

Figure 1: Chemical structure of the Rough LPS chemotypes Ra EH100 and Rc J5. Adapted from Inagaki *et al.*[38] SUgars in red are not present in the Rc J5 LPS chemotype.

Mixed monolayers of Rough LPS chemotypes and d_{62}-DPPC were studied in neutron reflectivity (NR) and Brewster angle microscopy (BAM) experiments in order to characterize their behavior at the air/liquid interface.[39] Monolayers were also used to study the kinetics and magnitude of peptide interactions with each LPS chemotype following subphase injection, and in order to determine the length of time needed to allow equilibrium to be reached in the subsequent NR studies, following challenge by AMPs.[13,40–42]

These biophysical observations on the role of LPSs in the membrane models were devised to elucidate the stabilizing role of different rough LPS chemotypes on the OM structure as well as their influence on the activities of LL37 and LFb.

2 Experimental section.

2.1 Materials.

Rc LPS from *E. coli* J5 (impurities: protein 1.4%, nucleic acid 0.340%), was obtained from Merck KGaA (Darmstadt, Germany) and was used without further purification. LPS from *E. coli* EH100 was obtained from Sigma-Aldrich Ltd. (Dorset, U.K.) and used after purification following the method described elsewhere.[30] LL37 peptide was obtained from GenScript USA Inc. (Piscataway,USA) with a purity >94%. The LFb peptide was obtained from Alpha Diagnostic International Inc. (Sant Antonio, USA) with a purity >90%. Both peptides were used as supplied. Deuterium oxide D_2O 99.990 atom % D and $MgCl_2$ anhydrous were also supplied by Sigma Aldrich Ltd. The lipids, hydrogenated 1,2-dipalmitoyl-sn-glycero-3-phosphocholine (h-DPPC) and chain deuterated 1,2-dipalmitoyl-d_{62}-sn-glycero-3-phosphocholine (d_{62}-DPPC) were obtained from Avanti Polar Lipids (Alabaster, USA) and used without further purification. Chloroform and methanol were obtained from Fisher Scientific (Loughborough, U.K.). Ethanol (99%) was obtained from VWR International (Lutterworth, U.K.). All the organic solvents used were of analytical grade or better. The ultrapure water at 18.2 $M\Omega \cdot cm$ was obtained from a Purelab Ultra machine from ELGA Process Water (Marlow, U.K.). Whatman chromatographic paper No.1 from Merck KGaA (Darmstadt, Germany) was used to produce the Wilhelmy plates required for the monolayer surface pressure measurements.

2.2 Solid state ^{2}H NMR measurements.

The phospholipid/LPS mixtures used to produce the multilamellar liposomes for the ^{2}H NMR experiments contained 30 or 40 mol% d_{62}-DPPC in lieu of the equivalent amount of h-DPPC. The pure DPPC lipid mixture contained 40 mol% d_{62}-DPPC with 60 mol% h-DPPC. The lipid mixtures Eh-20 and J5-20 contained 20 mol% of either Ra EH100 LPS or Rc J5 LPS respectively, 30 mol% of d_{62}-DPPC and 50 mol% h-DPPC, giving a total mass of 4 mg with 80 mol% phospholipid and 20 mol% LPS. A summary of the acronyms used to

Table 1: Acronyms used for each sample in the experiments and relative compositions.

Experiment	Acronym	Composition (in mol%)
ssNMR	DPPC	40% d_{62}-DPPC [a] + 60% h-DPPC[b]
	Eh-20	30% d_{62}-DPPC + 50 % h-DPPC + 20% LPS EH100
	J5-20	30% d_{62}-DPPC + 50 % h-DPPC + 20% LPS J5
Langmuir monolayers	DPPC	100% h-DPPC
	Eh-20	80% h-DPPC + 20% LPS EH100
	J5-20	80% h-DPPC + 20% LPS J5
Neutron reflectivity	h-Eh-20[c]	80% h-DPPC + 20% LPS EH100
	h-J5-20	80% h-DPPC + 20% LPS J5
	d-Eh-20[c]	80% d_{62}-DPPC + 20% LPS EH100
	d-J5-20	80% d_{62}-DPPC + 20% LPS J5

[a] chain deuterated 1,2-dipalmitoyl-d_{62}-sn-glycero-3-phosphocholine (d_{62}-DPPC); [b] hydrogenated 1,2-dipalmitoyl-sn-glycero-3-phosphocholine (h-DPPC); [c] *h* or *d* at the beginning of the acronym are used to indicate respectively the use of h-DPPC or d_{62}-DPPC in the mixture

describe the lipid/LPS mixtures used in the experiment and their relative compositions is reported in Table 1. The composition of the vesicles in consistent with the composition of the monolayers used in the Langmuir monolayers and NR experiments. Where necessary, at the mixing stage, the peptides were added to the lipid mixture solutions to give final lipid/peptide molar ratios of either 50:1 or 100:1, from solutions prepared in ethanol. The mixtures were bath-sonicated for 5 minutes at 22°C temperature in an Elmasonic P ultrasonic bath (Elma Hans Schmidbauer GmbH & Co. KG, Singen, Germany) at a frequency of 37 kHz and 320 W power to ensure the homogenization of the lipids. The organic solvents were thoroughly evaporated under vacuum by the use of a Buchi R-210 rotory evaporator (Buchi Labortechnik AG, Flawill, Switzerland) connected to a KNF Lab Neuberger Laboport Diaphragm Vacuum Pump UN840.3 FTP (KNF Neuberger UK, Witney, UK) and equipped with a Buchi waterbath at 40°C , and then by storage in a desiccation chamber under vacuum for 12 hours. The dry lipid/LPS and lipid/LPS/peptide films were resuspended in 4 mL of 10 mM TRIS, 1 mM $MgCl_2$, pH 7.4 buffer to give a final total lipid concentration of 1 mg/mL. At this stage, to ensure the complete resuspension of the films, they were placed in an ultrasonic bath for 10 min at 22°C with constant sonication at 37 kHz and 320 W

power. In order to produce multilamellar liposomes the lipid suspension was subjected to 5 freeze-thaw cycles[43] by freezing the samples in liquid nitrogen forming a thin layer on the sides of the flask and then thawing the samples in a water bath at 40°C . The resulting suspension was centrifuged at 15000×g for 30 min to obtain a dense white pellet containing the liposomes.[37]

The pellets were transferred into a Bruker 4 mm Magic Angle Spinning (MAS) rotor. Deuterium quadruple echo experiments on a Bruker Advance 400 NMR spectrometer were performed at 61.46 MHz using a 4 mm MAS probe. The spectral width of 100 KHz was used with a recycle delay of 0.25 s, echo delay of 100 μs, acquisition time of 2.6 ms and 90° pulse lengths of 3 μs. Experiments were performed at 45°C , just above the L_β to L_α phase transition temperature of the DPPC and LPSs, to ensure that the acyl chains were in the fluid phase.[44] The acquired spectra were dePaked using the Amix software package (Bruker) to determine the quadrupolar splittings[36] and then fitted with the software PeakFit using mixed Gaussian-Lorentzian fit (r^2>0.997) to obtain the smoothed deuterium order parameter (S_{CD}) profile plotted against the carbon number in the chain.[37] 2H NMR experiments were performed once only since each experiment requires 12-24 hrs of FID accumulation. The time averaging and high sensitivity of the 2H quadrupolar coupling ensures a highly precise measurement where even small differences in lipid acyl chain order are detectable. Importantly, the shape of the powder pattern obtained is an essential internal control as, in addition to the order parameter obtained from the quadrupolar coupling, it indicates that the DPPC remains in a fluid lamellar phase. Details of the ssNMR data analysis are reported in the supporting information.

2.3 Langmuir monolayers at the air/liquid interface.

Pressure-Area ($P - A$) isotherm measurements were carried out at 22 on a Nima Langmuir trough 602A (Nima Technologies Ltd., Coventry, U.K.). Prior to use, the polytetrafluoroethylene (PTFE) surface of the trough was extensively cleaned with ethanol and chloroform. A clean Whilelmy plate (0.75 × 1.3 cm) was attached to the microbalance and dipped into

the aqueous subphase consisting of 1 mM $MgCl_2$ solution. The composition of the lipid or lipid/LPS mixtures are consistent with the ssNMR and NR experiments, and their relevant acronyms are reported in Table 1. The lipid or lipid/LPS mixtures were reconstituted by sonication in pure chloroform at a total concentration of 1 mg/mL (1.4 mM for DPPC and 0.75 mM for J5-20 and Eh-20 mixtures) producing an homogeneous suspension. For each isotherm, enough lipid suspension (approximately 70 μL) was added dropwise to the cleaned subphase surface in order to allow the monolayer to be formed and to reach its collapse point upon compression. After allowing 10 min for solvent evaporation, pressure-area ($P - A$) isotherms were measured during eight cycles of compression and expansion at a constant barrier speed of 35 cm^2/min whilst changes in surface pressure were constantly recorded and the monolayer was compressed until its collapse point was reached.

The limiting molecular area for each monolayer was calculated from the $P - A$ isotherm from the tangent of the $P - A$ isotherm at 30 mN/m. Since the monolayers were formed by mixtures of lipids and LPS, the additive area per molecule rule was employed according to $A_{tot} = A_1 \cdot N_1 + A_2 \cdot N_2 + A_n \cdot N_n \ldots$, where A_{tot} is the area per molecule of the mix whilst A_n and N_n are respectively the area per molecule and the molar percentage of each component within the mixture. The compressibility modulus (E_S) is calculated according to the equation[45,46]

$$E_S = -A\left(\frac{d\pi}{dA}\right) \tag{1}$$

where A is the area per molecule and $d\pi/dA$ is the slope of the isotherm at a defined surface pressure. The plot E_S *vs surface pressure* allows an appreciation of the effect of the addition of 20 mol% of either EH100 or J5 LPS in h-DPPC monolayers.[47] A liquid condensed state is characterized by E_S values within 100-250 mN/m whereas a solid state is characterized by E_S values above 250 mN/m.[48]

2.4 Brewster angle microscopy (BAM).

The Brewster angle microscopy (BAM) measurements were performed at the Partnership for Soft Condensed Matter facility at the *Institut Laue-Langevin* (ILL) using an Accurion Nanofilm EP3 Brewster angle microscope. Polarized light from a He-Ne laser was specularly reflected from the air/liquid interface monolayer at the Brewster angle of 53°[49,50] and was detected by a CCD on which images of the lateral structure of the interface were captured. Each of the pure lipid or lipid/LPS monolayers tested were spread on a aqueous subphase consisting of a 1 mM $MgCl_2$ solution at 22°C , as previously described for the Langmuir monolayer experiments. The film was compressed at a constant barrier speed of 35 cm^2/min and images where taken at surface pressures of 10, 15, 25 and 35 mN/m.

2.5 Interaction studies of LL37 and LFb peptides and mixed DPPC/LPS monolayers.

The air/liquid interface monolayer technique was used to investigate the interaction of peptides and mixed monolayers containing 80 mol% h-DPPC and 20 mol% of either Ra EH100 LPS or Rc J5 LPS. The acronyms and compositions relevant to each monolayer are reported in Table 1. The experiment was performed at 22°C using the Nima PS4 surface pressure microbalance with a 50 mm diameter fluorinated ethylene propylene (FEP) Petri dish (Welch fluorocarbon Inc., Dover, U.K.) positioned on a magnetic stirring plate. The Petri dish was filled with filtered 1 mM $MgCl_2$ solution giving a final subphase volume of 15 mL. A 5 mm magnetic stirring bar was placed into the subphase into which a Whilelmy plate attached to the pressure sensor was dipped. Prior to monolayer deposition, a syringe containing 100 μL of $\sim$70μM peptide solution was fixed in position with its needle penetrating into the subphase below its surface. Mixtures of LPS and lipid in chloroform were spread dropwise onto the cleaned subphase surface until a pressure of approximately 32 mN/m was achieved. The surface pressure was recorded with constant slow stirring of the subphase, with the magnet speed set at its minimum in order to avoid a variation of pressure greater than 0.2 mN/m.

The monolayer was allowed to equilibrate until the surface pressure reached a plateau before carefully injecting the 100 μL of peptide solution into the subphase resulting in an excess bulk concentration of peptides (approximately double the lipid concentration), in order to ensure their interaction with the monolayer. The change in pressure over time was recorded and the isotherms produced were fitted with a Hill equation $y = Pmax \cdot [t^n/(k^n + t^n)]$ to obtain kinetic parameters for the maximum change in pressure (P_{max}), the Hill coefficient (n) and the time needed to obtained half of the maximum increase in pressure (k). In particular k is inversely proportional to the rate of pressure increment, hence lower values of k refer to faster interactions with a monolayer.

2.6 Neutron reflectivity of mixed LPS/DPPC monolayers at the air/liquid interface and their interaction with antimicrobial peptides.

The experiments were performed on the FIGARO reflectometer beam line at the Institut Laue Langevin high-flux reactor in Grenoble (France).[51] A custom-made reduced-area Teflon Langmuir trough with a 50 mL subphase volume was placed on an active, variable-height, anti-vibration stage. After the initial alignment using neutrons, the height of the air-liquid interface was automatically adjusted using a height alignment laser linked to the sample stage to ensure that the neutron footprint remained on the sample throughout the measurements in the eventuality of subphase evaporation. The incoming neutron beam had a usable wavelength range between 2 Å and 20 Å and grazed the subphase from above at two incident angles (0.624° and 3.78°) to access a range of momentum transfer perpendicular to the surface (Qz) from 0.007 to 0.4.

The NR measurements were carried out on mixed lipid/LPS monolayers composed of 20 mol% LPS and 80 mol% phospholipid, to be consistent with the previous experiments. The Eh-20 and d-Eh-20 coded monolayers refer to mixtures containing respectively 80 mol% of either h-DPPC or d_{62}-DPPC and 20 mol% Ra EH100 LPS. The J5-20 and d-J5-20 coded

monolayers refer to mixtures containing respectively 80 mol% of either h-DPPC or d_{62}-DPPC and 20 mol% Rc J5 LPS. Table 1 reports the acronyms for each monolayer used and their composition. The choice of h-DPPC or d_{62}-DPPC was dependent upon the desired isotopic contrast. The chain-deuterated d_{62}-DPPC was mixed with the LPS chemotypes to be used with either D_2O or air contrast matched water (ACMW) (8% v/v D_2O in H_2O) subphase in order to highlight the properties of the hydrogenated headgroups and the acyl chain region of the monolayers, respectively. The h-DPPC was used on D_2O subphase to focus on the properties of the whole monolayer. Both D_2O and ACMW subphases always contained 1 mM $MgCl_2$ and all measurements were made at 22°C .

The monolayer mixtures were suspended in chloroform after extensive sonication and were deposited dropwise onto a cleaned subphase using a micro-syringe (Hamilton Co. Europe, Bonaduz, Switzerland). The chloroform was allowed to evaporate for 10 min and the monolayers were compressed a constant rate of 15 cm^2/min until a lateral pressure of 30 mN/m was achieved. The barriers were then kept fixed at a constant area and the monolayer was allowed to equilibrate and reach a stable pressure, determined by the formation of a plateau on the $P - A$ isotherm. A concentrated peptide solution of either LL37 or LFb was carefully injected into the subphase by the use of a small syringe to transfer the peptide into the subphase resulting in a final peptide concentration of $\sim$1.6 μM. The interaction between the peptides and the monolayer was allowed to progress by diffusion until a surface pressure plateau was reached.

The acquisition of the NR profiles was performed during the post-interaction plateau phases of the monolayers as defined by the $P - A$ plot. The NR profile data for each monolayer mixture with different isotopic contrasts in the absence or presence of either LL37 or LFb peptides were reduced and the data from the different contrasts were simultaneously fitted using a custom model in the RasCAL analysis software.[52]

For the purposes of data fitting, the interface was divided into layers consisting of a chain region layer composed of the hydrophobic acyl chains only, an the inner headgroup layer composed of the glucosamine (GlcN) and the 3-deoxy-D-mannooctulosonic acid (Kdo) residues

of LPS together with the headgroup of DPPC, and the carbohydrates constituting the core of the LPS beyond the Kdo residues were considered to form an outer headgroup layer (Figure 1). The amount of solvent present in the chain region, which was considered to be negligible, together with the scattering length density (SLD) of the fully hydrogenated and mixed hydrogenated/deuterated chains were all held constant during the analysis routine. The calculation of the total SLD of the chains considered the ratio between the lipid (d_{62}-DPPC or h-DPPC) and the hydrogenated LPSs (respectively 80 to 20 molar ratio) and their relative SLDs. It was found that the total SLDs of the fully hydrogenated and mixed H/D chain regions were respectively -3.9×10^{-7} and 5.88×10^{-6} $Å^{-2}$. Estimation of the SLDs of the molecules used are reported in the Supporting Information.

3 Results

3.1 Solid state ^{2}H NMR.

Solid state ^{2}H NMR experiments were carried out on liposomes composed of pure h-DPPC/d_{62}-DPPC alone and mixed with either EH100 or J5 LPS in the designed Eh-20 and the J5-20 lipid/LPS mixtures at 45°C in the presence of 1 mM $MgCl_2$. The addition of the two LPS chemotypes induced a limited broadening of the ^{2}H NMR spectrum of h-DPPC (Figure 2 A) suggesting the conferring of an ordering effect on the lipid bilayer above the T_m of DPPC. The ordering effect induced by J5 LPS is of greater magnitude than the effect induced by EH100 LPS, as shown by the smoothed order parameter S_{CD} in Figure 2 C. Within the bilayer, J5 LPS induces an ordering effect which is distributed along the carbon chains of d_{62}-DPPC, from the distal carbons to the ones closer to the headgroup. The influence of EH100 LPS on the ordering of d_{62}-DPPC chains is more subtle and it is mostly limited to the carbons closer to the headgroup region.

The effect of the peptides LL37 and LFb on the order state of the bilayers at a lipid:peptide molar ratio of 50:1 was investigated in the same conditions mentioned above. LL37 scarcely

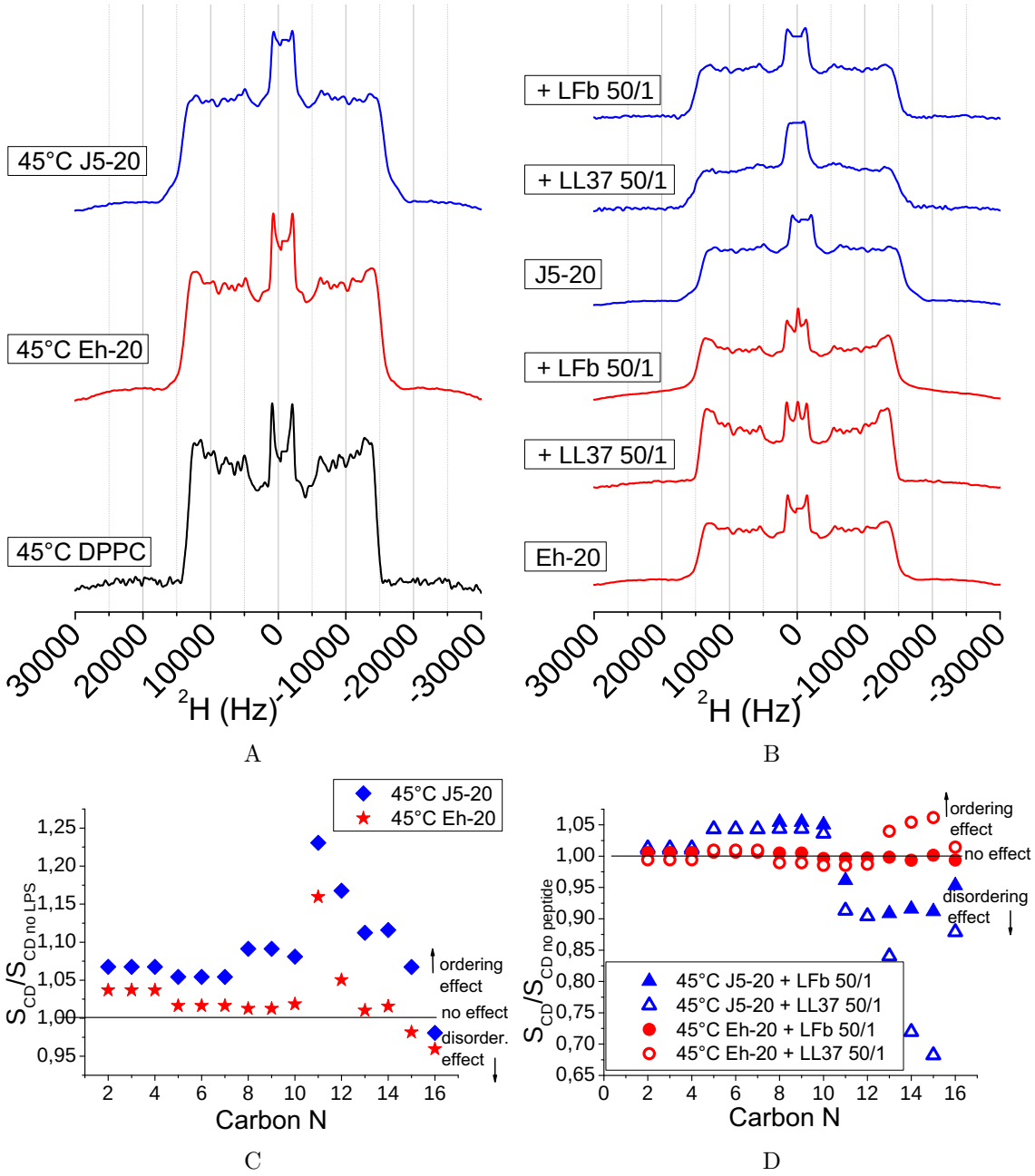

Figure 2: (A) ^{2}H NMR analysis at 45°C of the pure DPPC (black), Eh-20 (red) and J5-20 (blue) liposomes and in the presence or absence of the peptides LL37 and LFb (B) at a lipid:peptide ratio of 50:1. Calculated smoothed order parameters (S_{CD}) relative to profiles for the corresponding LPS-free liposomes (C) and peptide-free liposomes (D).

modifies the ^{2}H NMR spectrum of the liposomes composed of the Eh-20 mixture, whereas it induces more significant changes in the liposomes composed of the J5-20 mixture, with an appreciable broadening of the powder spectrum of d_{62}-DPPC (Figure 2 B) and a greater deviation of the S_{CD} values from the state without the presence of the peptides ("no effect" line in Figure 2 D). The S_{CD} plot in Figure 2 E shows that Eh-20 mixture order parameter increases up to 1.05 upon addition of LL37 in the distal carbon of the chains, whilst the J5-20 mixture signal in the presence of the peptide produced an increase of relative S_{CD} of the central carbon of the chains (up to 1.05) and a decrease (up to 0.70) in the distal carbon of the chains (Figure 2 D).

The LFb peptide had no noticeable effects on the ^{2}H NMR spectrum of the Eh-20 bilayer and the modifications induced to the ^{2}H NMR spectrum of J5-20 are less marked than the LL37 case (Figure 2 B). The S_{CD} profile of the Eh-20 liposomes in the absence or presence of the peptide LFb at a lipid:peptide molar ratio of 50:1 are identical (Figure 2 E, Supporting information). The increase of the relative S_{CD} values of the J5-20 mixture bilayer in the presence of LFb shows that the peptide induces a slightly increased ordering (up to 1.05) in the bilayer at the central carbons and a disordered state (up to 0.90) at the carbons closer to the centre of the bilayer (Figure 2 D).

For a comparison, the DPPC liposomes were challenged by the peptides LL37 and LFb at the same conditions. LFb under the lipid:peptide ratio of 50:1 noticeably reduced the S_{CD} values of DPPC liposomes; the disordering effect was marked on the carbons closest to the headgroup region (Figure 2 B, Supporting information). LL37 did not allow the formation of liposomes when pre-mixed with the h-DPPC/d_{62}-DPPC lipids; even at the lower peptide concentration it was not possible to obtain a liposome pellet probably due to its detergent-like activity.[53] Though the bilayer disordering effects of LL37 and LFb are different, with LL37 markedly more potent, the effects of the two peptides on LPS containing liposomes are consistent with previous studies which showed a greater cytoplasmic activity and lower MIC of LL37.[54] The data indicate that Ra EH100 may be more effective at protecting the bilayer from the disordering effects of AMPs due to the steric hindrance of its larger headgroup or it

may be less sensitive to the perturbation activity of AMPs due to its pre-existing ordered state of the bilayer.[55] These hypotheses were further examined in the interaction studies using neutron reflectivity.

3.2 Langmuir monolayers at the air/liquid interface.

The $P - A$ isotherms of pure h-DPPC and mixed monolayers containing 80 mol% h-DPPC and 20 mol% of either LPS EH100 or LPS J5 on an aqueous subphase of 1 mM $MgCl_2$ solution at 22°C , are shown in Figure 3 A whilst the values of the calculated area per molecule of each component are reported in Table 2. The isotherms for pure h-DPPC obtained in this experiment are comparable with those observed in previous experiments[56] and present the characteristic liquid expanded (LE) to liquid condensed (LC) phase transition occurring below 10 mN/m in the presence of Mg^{2+} ions.[57,58] In consideration of the additive rule for the area per molecule within a mixed monolayer the resultant area per molecule of the single components EH100 LPS and J5 LPS are thus respectively 175.1 and 119.7 Å^2 assuming ideal mixing with the DPPC (Table 2). The addition of 20 mol% of either LPS EH100 (Eh-20 monolayer) or LPS J5 (J5-20 monolayer) to h-DPPC monolayers removed the LE-LC phase transition of h-DPPC and the shape of the curve from the gaseous to a more condensed phase is gradual (Figure 3 A) as observed in other experiments containing mixed h-DPPC/LPS ratios.[59,60] A detailed observation of the three isotherms (Figure 3 A) in the liquid condensed

Table 2: Area per molecule and compressibility modulus E_S for each monolayer at 22°C at 30 mN/m lateral pressure on subphase of 1 mM $MgCl_2$ solution and relative standard deviations (calculated from at least 3 replicates).

Monolayer	LPS type	Area per molecule (Å^2/molecule)	Compressibility modulus E_S (mN/m)
h-DPPC	—	57.5 ±2.4	250 ± 45
J5-20	LPS J5	119.7 ±7.3	175 ± 38
Eh-20	LPS EH100	175.1 ±13.0	168 ± 12

phase, between ∼10 and ∼20 mN/m, shows that the LC phase of the h-DPPC isotherm is steeper than the LC phase of the curves of the monolayers containing LPS, suggesting

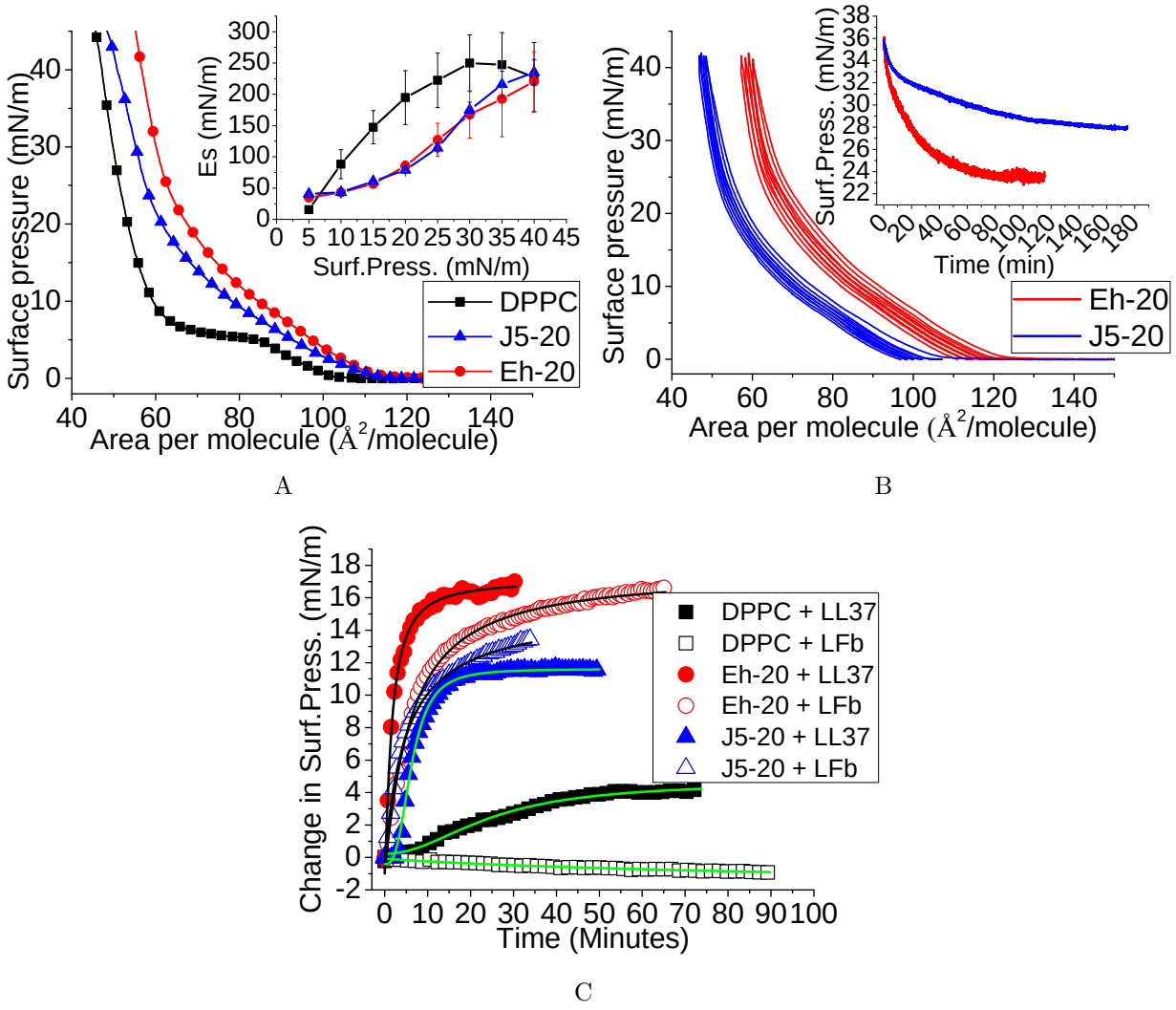

Figure 3: Monolayers at the air/liquid interface of DPPC, J5-20 and Eh-20 on subphase containing 1 mM $MgCl_2$ at 22°C (A) $P-A$ isotherms. Inset: surface compressive modulus E_S of the same system at different pressure. (B) Monolayers cycled up to the target pressure of 40 mN/m. Inset: monolayers stability at constant barrier area over time. (C) Representative curves of the interaction of LL37 and LFb peptides with monolayers after subphase injection fitted with the Hill function (green or black lines). Injection into the subphase occurred at Time=0. At least three sets of experiments for each system were recorded and the average kinetic parameters were calculated and reported in Table 3.

that in this phase the pure h-DPPC monolayer is less compressible while the addition of the LPS chemotypes makes the film more fluid and elastic, as reported by lower compressibility modulus (E_S) values in Table 2. In the region of the LC-solid phase, at surface pressures above 20 mN/m, the h-DPPC monolayer and the Eh-20 monolayer present a steeper isotherm curve compared to the monolayer containing Rc J5 LPS, suggesting that during this phase only, J5 LPS has a greater fluidizing effect on the h-DPPC monolayer.

The calculation of the surface compressional modulus (C_S) from the isotherms allows a better understanding of the compressibility of the monolayers and the effect of the addition of LPS to h-DPPC films.[45,46] Pure h-DPPC monolayers enter the liquid condensed state right above the surface pressure of 10 mN/m and the rapid E_S increase suggests a low compressibility of this monolayer which reaches the condensed state at 30 mN/m pressure equivalent to the lateral pressure of biological membranes.[42] Both LPS chemotypes elicit a decrease in the E_S values of h-DPPC isotherms allowing the formation of a liquid expanded phase up to the surface pressure of 25 mN/m, the pressure at which the monolayers entered the liquid condensed state. Neither of the mixed monolayers Eh-20 and J5-20 show the formation of a clear solid phase, according to the values of the compressibility modulus. This evidence suggests a fluidizing effect of the LPSs on h-DPPC monolayers at 22°C , despite the data obtained from the isotherms which indicate the reaching of a more condensed state. The disordering effect of LPS on h-DPPC monolayers has been observed before in LB experiments with h-DPPC and smooth LPS[60] and solid state NMR experiments containing h-DPPC and rough LPS from *E. coli*, below the T_m of DPPC.[61] A detailed investigation of the curves in the inset of Figure 3 A, despite the considerable variability of the data, shows that over the surface pressure of 30 mN/m (Table 2) the compressibility of monolayers containing J5 is lower than the compressibility of monolayers containing EH100, something not apparent from the direct observation of the isotherms. The data suggest that LPS J5 induce a greater ordering effect of the DPPC monolayer compared to the LPS EH100.

3.2.1 Stability study of monolayers at the air/liquid interface

In order to define the stability of the mixed monolayers composed of 80 mol% DPPC and 20 mol% of either EH100 or J5 LPS at 22°C on an aqueous subphase of 1 mM $MgCl_2$ solution, the films were subjected to multiple cycles of compression and expansion and the surface pressure was continuously recorded. The cycled isotherms of the mixed monolayers do not overlay completely (Figure 3) and show the presence of some hysteresis, possibly caused by the loss of lipid and LPS molecules into the subphase which results in a lower area per molecule at high pressures. The monolayer stability under the same subphase conditions at 22°C was studied at a constant surface area measuring the change in surface pressure over time as well. The isotherms reported in the inset of Figure 3 B show that the monolayer Eh-20 reached a final pressure of approximately 24 mN/m where it stabilizes within two hours, whilst the J5-20 monolayer took longer to equilibrate to a final pressure of approximately 28 mN/m after more than three hours. The equilibration process may result from a combination between the packing of the lipid and LPS molecules into a stable monolayer and a partial loss of these materials into the subphase.

3.3 Brewster angle microscopy (BAM).

The BAM technique has been extensively used in qualitative studies of lipid monolayers[62–64] as well as monolayers composed of Rc LPS from *E. coli*[65] and to investigate the insertion of proteins into lipid films.[66,67] In this study BAM images at 22°C on water subphase containing 1 mM $MgCl_2$ were taken at different lateral pressure for the monolayers h-DPPC, Eh-20 and J5-20 in order to investigate the structural modifications induced by the presence of 20 mol% of either EH100 or J5 LPS in h-DPPC films (Figure 4). The h-DPPC monolayer developed the characteristic cluster pattern with the formation of white lobed-like domains of lipids typical of the LE-LC transition state between 5 and 10 mN/m.[63] The compression of the h-DPPC monolayer over the LE-LC transition shows the aggregation of the condensed

domains until, upon further compression above 14.5 mN/m, they disappear when the film is compressed up to its solid phase. During the solid phase no islands are visible because the repulsive forces between the different clusters are overcome by the lateral pressure and the film presents a homogeneous surface.

The J5-20 monolayer (Figure 4) at a lateral pressure below 15 mN/m presents domains which are probably formed by h-DPPC in the liquid condensed state, whereas the remainder of the monolayer is still in a liquid expanded state (Figure 3 A). The presence of LPS J5 modified the shape of the domains of h-DPPC suggesting a close interaction between the amphiphiles. A similar effect was observed for Re LPS and h-DPPC monolayers in the presence of Ca^{2+}, using a fluorescence microscopy technique on monolayers at the air-water interface.[59] Above 15 mN/m the film enters the liquid condensed phase and the image becomes more homogeneous, but still some clusters are visible up to 35 mN/m. The existence of domains at every surface pressure suggests that the J5-20 monolayer is in constant coexistence between two phases corresponding to the absence of a defined phase transition of the $P - A$ (Figure 3 A) and in-line with the compressibility modulus calculations.

The Eh-20 monolayer is characterized by the absence of domains at low surface pressure up to 10 mN/m, suggesting a homogeneous gas phase. This homogeneity may suggest that EH100 has a fludizing effect on h-DPPC, removing completely the characteristic LC domains of DPPC. The nucleation visible at 15 mN/m suggest the formation of a coexistent LE-LC phase, which is maintained up to 35 mN/m. The actual shift of the phase transition of h-DPPC towards higher pressure supports the hypothesis of a disordering effect of EH100 on the h-DPPC monolayer. The dashed white line on the picture of Eh-20 monolayer at 35 mN/m (Figure 4) highlights a possible rupture of the monolayer, indicating the proximity to its collapse.

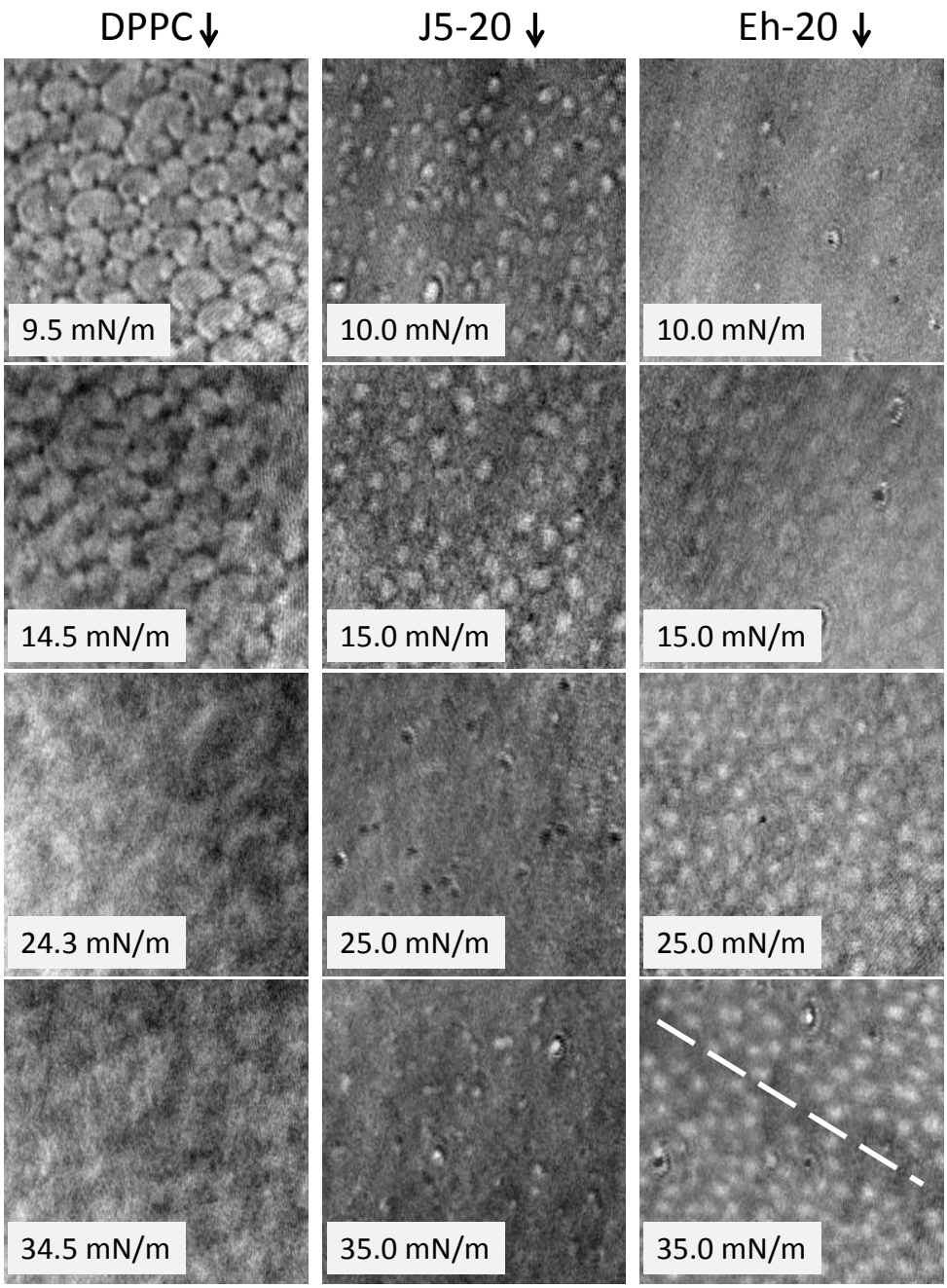

Figure 4: BAM images of $P - A$ isotherms at 22°C on water subphase of 1 mM $MgCl_2$ solution of pure h-DPPC, Eh-20 and J5-20 monolayers.

3.4 Interaction studies of LL37 and LFb peptides and mixed DPPC/LPS monolayers.

The mixed h-DPPC/LPS monolayers spread on 1 mM $MgCl_2$ solution at 22°C held at a constant area per molecule were challenged by a subphase injection of the two peptides LL37

and LFb. The resultant changes in surface pressure of the monolayers were recorded and the data monitored over time (Figure 3 C). The initial lateral pressures of the pure DPPC, Eh-20 and J5-20 monolayers after equilibration were respectively 29±3 mN/m, 25±4 mN/m and 28±2 mN/m. The curves were fitted with a Hill function and the parameters $1/k$, P_{max} and n were calculated (Table 3).

The presence of 20 mol% of either EH100 or J5 LPS in the monolayer of h-DPPC allows for a rapid binding of LL37, characterized by a linear increase in the surface pressure already in the initial 5 minutes of interaction (Figure 3); the rate of surface pressure increase $1/k$ is $2.80e^{-3}$ and $5.3e^{-3}$ respectively for J5-20 and Eh-20 monolayers, hence the increase of surface pressure induced by LL37 on Eh-20 monolayer is faster than in the case of the J5-20 monolayer showing that the presence of Ra EH100 LPS results in a monolayer more accessible to the penetration of the peptide. Nevertheless the standard deviation for the latter value should be considered. For the same reason, LL37 induces a greater total surface pressure change in the Eh-20 monolayer than in the J5-20 monolayer, as reported by the $PMax$ values which were respectively 18.42 and 11.24 mN/m. LL37 binds less with the monolayer composed of pure h-DPPC (Figure 3 C) as revealed by a slow and gradual surface pressure change with a $1/k$ rate value noticeably lower than the value in the presence of LPSs in the mixture; the extent of the surface pressure modification is also lower and the P_{max} reaches only 3.37 mN/m and approaches a plateau after one hour. The LFb peptide injection yields $1/k$ values of $1.75e^{-3}$ and $2.43e^{-3}$ respectively for the J5-20 and Eh-20 monolayer (Table 3) suggesting a faster initial interaction of LFb in the presence of the Ra EH-20 LPS, although the standard deviation of the former parameter has to be considered. Interestingly the P_{max} values for the monolayers containing EH100 (17.42 mN/m) are slightly higher than for the monolayer containing J5 LPS (15.56 mN/m) confirming the greater susceptibility to peptide penetration of monolayers composed of EH100 LPS. LFb showed no interaction with h-DPPC, and the monolayer pressure remained unchanged.

In general LFb seems to induce a greater P_{max} change than LL37 on the J5-20 monolayer, and the Eh-20 monolayer seems to be more susceptible than J5-20 to the penetrating activity

of the peptides.

Table 3: Kinetic parameters and standard deviations obtained from the Hill plots of the isotherm of the three monoayers at 22°C on 1 mM $MgCl_2$ solution after subphase injection of either LL37 or LFb peptides. $1/k$ is proportional to the rate of pressure increment, P_{max} is the maximum pressure reached.

	Parameters	DPPC	J5-20	Eh-20
LL37	P_{max} (mN/m)	3.22 ± 1.41	11.24 ± 1.28	18.40 ± 1.26
	$1/k$ (min^{-1})	$1.03e^{-3}$ ± $3.13e^{-4}$	$2.80e^{-3}$ ± $2.3e^{-3}$	$5.3e^{-3}$ ± $3.5e^{-3}$
	n	3.37 ± 1.37	2.36 ± 0.59	1.29 ± 0.27
LFb	P_{max} (mN/m)	—	15.56 ± 1.34	17.42 ± 0.11
	$1/k$ (min^{-1})	—	$1.7e^{-3}$ ± $1.4e^{-4}$	$2.43e^{-3}$ ± $2.05e^{-4}$
	n	—	0.86 ± 0.17	0.88 ± 0.27

3.5 Neutron reflectivity of mixed LPS/DPPC monolayers at the air/liquid interface and interaction with antimicrobial peptides.

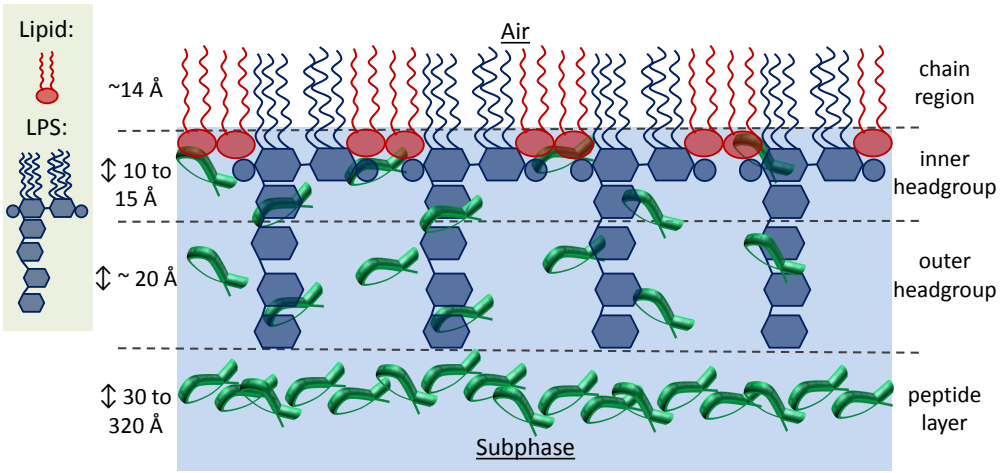

Figure 5: Schematic diagram showing the molecular contents of the various monolayer subdivision assumed in the NR data analysis. Peptide is shown distributed between the subphase and each of the different headgroup layers.

NR studies of the interaction of AMPs with LPS-containing monolayers provided a useful and reliable method to assess the likely interaction and the extent of permeation capacity of the peptides into Gram negative membrane mimetic systems.[40,41,68]

The fitting of the NR data (Figure 6 and 7) was constrained by fitting all the contrasts for each particular LPS chemotype simultaneously and ensured the reproducibility of the AMP/monolayer interaction. This approach ensured that the same amount of material was present across all fits for a particular monolayer type, where peptide molecules were allowed within the fit to replace water in the LPS head inner and outer region as well as forming a layer underneath the monolayer. The monolayer was divided into contiguous layers as shown schematically in Figure 5. The parameters obtained from this analysis of the NR data of the bilayers Eh-20 and J5-20 in the absence or presence of the peptides, either LL37 or LFb, are reported in Table 4.

The tail thickness values obtained for the mixed monolayers Eh-20 and J5-20 were both of 14 Å, which is comparable with the thicknesses obtained from experiments carried out on monolayers at the air/liquid interface of pure d_{62}-DPPC (16 Å)[69] and pure Rc J5 LPS (12 Å).[65] The tail-air roughness values suggest that the Rc J5 LPS induces the formation of a more ordered monolayer compared to the Ra Eh100 LPS, in accordance with the NMR results reported above. The similarity between the SLD profiles (Figure 6 and 7) in this region obtained for the deuterated and hydrogenated chains in both contrasts, D_2O and ACMW, suggest a limited penetration of both the peptides in the chain region of the monolayers. For the Eh-20 and J5-20 monolayers, the fitted thickness of the inner head group layer, taken to include the DPPC head group and the GlcN and the Kdo moieties moieties of the LPS core region (Figure 1), were 15 and 9.9 Å respectively. The data are comparable to the range set by previously published values of the DPPC headgroup layer thickness (9.3 Å) and the Rc J5 LPS inner headgroup layer thickness (14 Å).[65,69] Interestingly, the data gave no evidence of LL37 within the inner head group region of the J5-20 monolayer but a significant amount (14%), in this region in the Eh-20 monolayer. The converse was found to be the case for the LFb peptide, with 41.7% in the inner head group region of the J5-20 monolayer and none

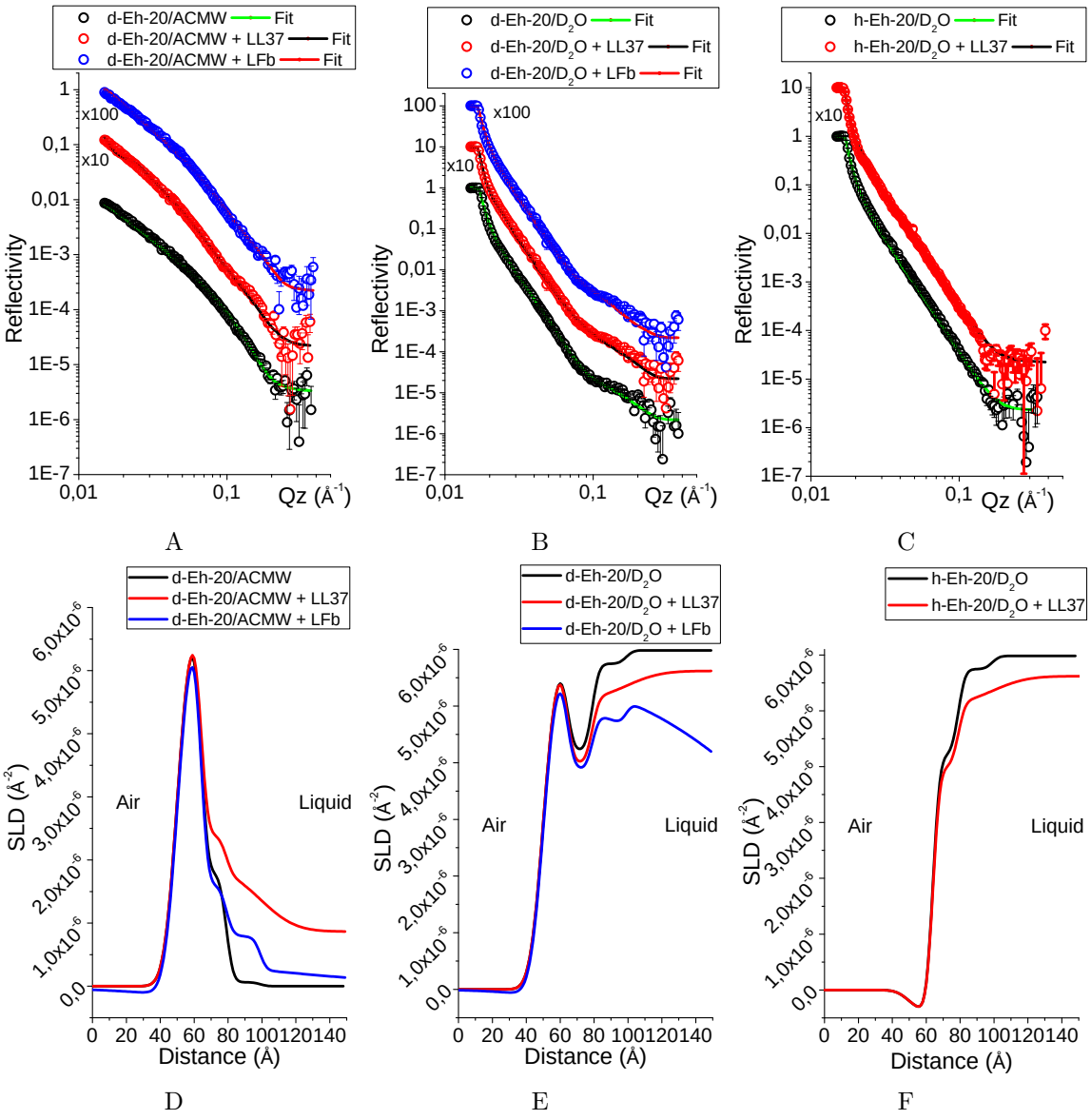

Figure 6: Neutron reflectivity and SLD profiles of deuterated Eh-20 monolayer on ACMW subphase (A,D) and D_2O subphase (B,E), and hydrogenated Eh-20 monolayer on D_2O subpahse (C,F). All the subphases applied contain 1 mM $MgCl_2$ and the experiments are carried out at 22°C . The NR data are collected before and after subphase injection of either LL37 or LFb peptides.

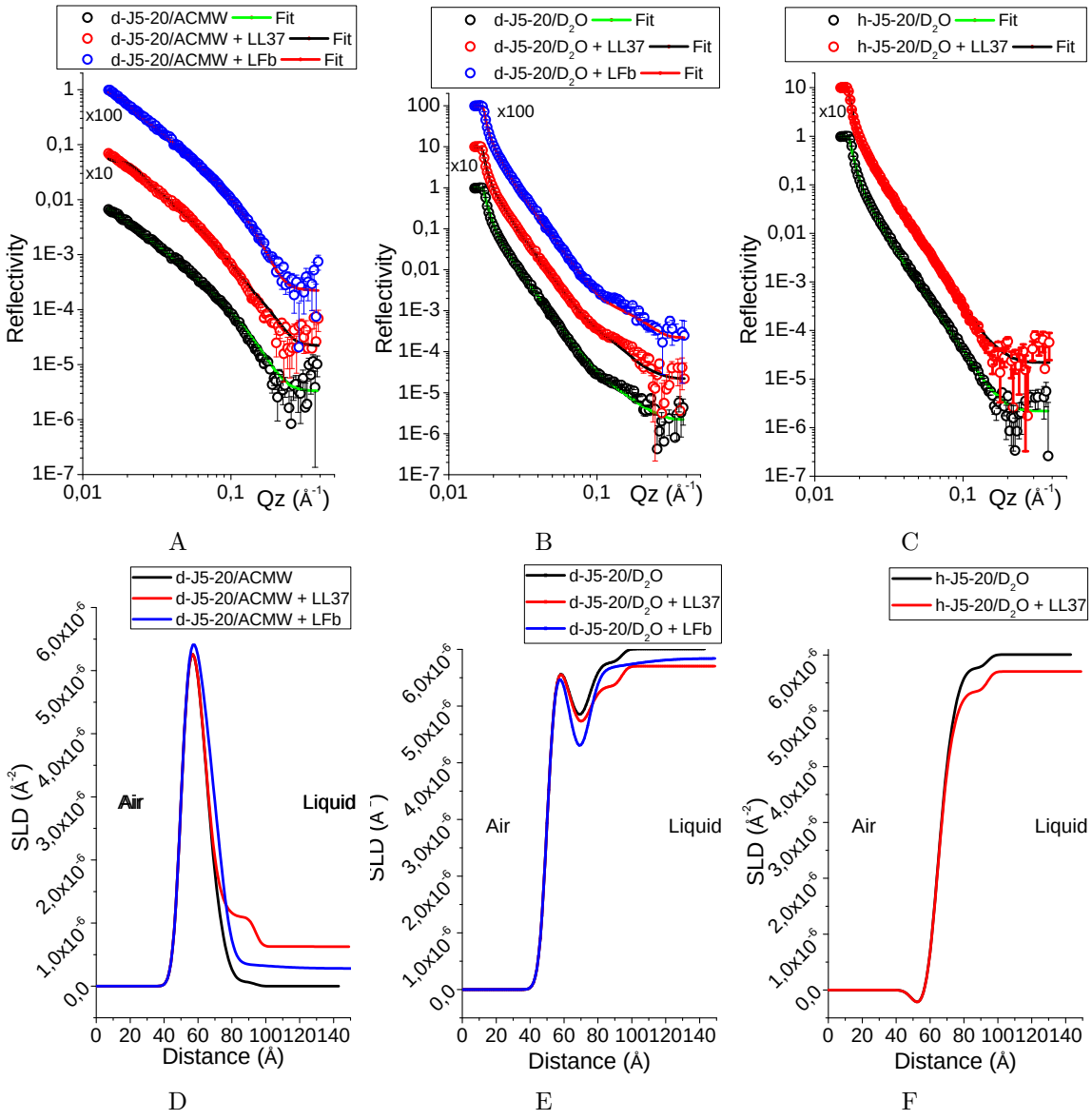

Figure 7: Neutron reflectivity and SLD profiles of deuterated J5-20 monolayer on ACMW subphase (A,D) and D_2O subphase (B,E), and hydrogenated J5-20 monolayer on D_2O subpahse (C,F). All the subphases applied contain 1 mM $MgCl_2$ and the experiments are carried out at 22°C . The NR data are collected before and after subphase injection of either LL37 or LFb peptides.

Table 4: Parameters obtained from the fitting of NR data of the mixed Eh-20 and J5-20 monolayers a the air/liquid interface at 22°C in the absence and presence of the peptides, either LL37 or LFb

		Eh-20	+ LL37	+LFb	J5-20	+ LL37	+LFb
Tail T[a]	(Å)	14.0±0.8			14.0±0.4		
Tail-Air R[b]	(Å)	6.1±0.5			2.9±0.5		
Inner Head T	(Å)	15.0±0.2			15.0±0.2		
Inner Head C[c]	(%)	59.6±6.5			59.6±6.5		
Peptide Inner Head	(%)	—	14.4±4.8	0.0±0.1	—	0.0±0.1	41.7±7.7
Inner Head SLD	($Å^{-2}$) x10^{-6}	3±0.2	3±0.2	3±0.2	2.9±0.21	2.9±0.21	2.9±0.21
Outer Head T	(Å)	20.0±0.5			20.1±1.3		
Outer Head C	(%)	5.0±0.9			5.0±0.5		
Peptide Outer Head	(%)	—	40.6±8.3	23.7±5.7	—	22.8±7.1	8.1±0.5
Outer Head SLD	($Å^{-2}$) x10^{-6}	1.25±0.01			1.3±0.04		
Inner Head R	(Å)	3.2±0.4			4.4±0.5		
Head-Water R	(Å)	3.4±1.0	—	—	3.0±1.4	—	—
Head-Peptide R	(Å)	—	16.2±2.1	3.1±0.3	—	3.0±2.2	21.9±4.9
Peptide Layer T	(Å)	—	261.7±50.2	30.5±2.7	—	323.4±60.1	98.7±21.3
Peptide Layer C	(%)	—	19.3±4.9	12.7±7.2	—	13.9±10.2	5.9±3.6
Peptide Layer R	(Å)	—	80.0±3.2	19.3±9.9	—	79.0±1.6	57.4±34.0
Peptide SLD	($Å^{-2}$) x10^{-6}	—	4.5±0.01	4.1±0.01	—	4.5±0.01	4.1±0.01

[a] T=thickness; [b] R=roughness; [c] C=coverage.

found in the head group layer of the Eh-20 monolayer (Table 4). These findings accord with those from the interaction studies reported above. The outer headgroup layer thicknesses for the Eh-20 and J5-20 monolayers were respectively 20 and 20.1 Å. The headgroup layer thickness of the monolayer containing EH100 LPS was lower than the corresponding layer thickness value of 31 Å obtained from the NR investigation of asymmetric bilayers composed of DPPC and EH100 LPS[70] whereas the J5 LPS headgroup thickness was in agreement with published data by the same group.[70] In this region the presence of LL37 is more pronounced in both Eh-20 and J5-20 monolayers (respectively 40.6% and 22.81% presence) compared to the LFb peptide (22.81% and 8.1 %). Consistently with the adsorption studies both peptides seem to interact more with the Eh-20 than the J5-20 monolayer. LL37 shows a stronger perturbation of the monolayers containing Ra EH100 LPS, whereas LFb seems to have a greater effect than LL37 the monolayer containing Rc J5-20 LPS. The LL37 creates thicker and rougher peptide layers underneath both Eh-20 and J5-20 monolayers (Table 4), compared to LFb. LL37 forms oligomers which interact with membranes containing anionic lipids, however its activity is attenuated against more ordered lipid bilayers.[14] There is no evidence for the formation of aggregates or oligomers by LFb and this process has so far only been postulated by Hwang.[71] These experiments suggest that both peptides form peptide layers underneath the monolayers which may affect their interaction with the system. The absence of LL37 peptide in the Inner headgroup region of J5-20 monolayer may result from its confinement in the thick peptide layer, which slows down and reduces the partitioning of the peptide in the headgroup region. Whereas LFb, by forming a thinner peptide layer, is more available in the bulk and hence, without the steric hindrance provided by the extra outer sugar residues otherwise present in the Eh-20 monolayer, it acts more efficiently in the inner headgroup region of J5-20 and induces a rougher Headgroup-Peptide layer interface (21.9 Å) compared to LL37 (only 3.0 Å).

4 Discussion

The experiments performed for this study on mixtures of 80% d_{62}-DPPC and 20% Rough LPS, either Ra EH100 or Rc J5 LPS, showed that in bilayers LPS increases the order of DPPC hydrocarbon chains above its T_m (41°C) when the bilayer is in the fluid phase; whereas when the DPPC chains are more ordered, below their T_m, LPS exerts a disordering effect on the chain packing, by increasing the fluidity of the monolayer.[59–61] In this regard the mixed DPPC/LPS monolayers at 22°C , at a surface pressure of 30 mN/m on a subphase containing $MgCl_2$ showed a reduction of the E_S (Table 2) compared to the pure DPPC monolayer. The BAM experiments carried out at 22°C on monolayer systems showed how both LPS types abolished the typical DPPC LE-LC transition at low surface pressure possibly due to their fluidizing effect. However J5 partially allowed the formation of DPPC domains (or clusters) suggesting a coexistence of phases whereas EH100, due to its greater disordering effect, homogenised the mixed monolayer into a gas phase with no clusters. The LB experiments indicate that Rc J5 LPS induced a relatively higher ordering of the DPPC acyl chains, compared to the Ra EH100 LPS, in accordance with the neutron reflectivity studies presented here which showed that the monolayer containing LPS J5 possessed a lower roughness (Tail-Air roughness value). These findings and previous experiments carried out on different pure LPS chemotypes using FT-IR[72] and molecular dynamic simulations,[73] suggest that a shorter oligosaccharide region of LPS may induce a higher ordered state on DPPC acyl chains, thus increasing the stability of the OM mimetic. The disordering effect of the EH100 is most likely due to increased lateral repulsion between the LPS headgroups, which will be proportional to the length of the oligosaccharide moiety.[4] However, in the natural OM, where the phosphate groups of the LPS inner core region are assumed to be cross-linked by Mg2+ ions[4,72] this is likely to have a stabilising effect which compensates for the repulsion between adjacent oligosaccharide headgroups. Although this highlights a limitation in our DPPC-stabilised planar model, our results are nevertheless consistent with previous studies stressing the importance of balancing the steric and electrostatic forces within the OM for the maintenance of its stability and reduced permeability.[5]

The more fluid monolayers containing either Ra EH100 or Rc J5 LPS allow a stronger binding of the peptides LL37 and LFb than the ordered monolayer containing pure h-DPPC. The stronger fluidizing effect of LPS EH100 allowed a greater peptide interaction compared to the systems containing LPS J5, resulting in greater maximum change in surface pressure (P_{max}). Interestingly the model applied to the NR data indicates that both peptides form a layer underneath the monolayer, with LL37 forming a thicker peptide layer than LFb. The peptide layers formed by LL37 and LFb are thicker in the presence of the J5 LPS-containing monolayer. Because of their defined facial amphiphilicity, α-helical peptides are cosidered to be stronger membrane-active agents,[12] hence LL37 initially binds to the negative charges presented by the LPS at the interface of the membrane and is then likely to penetrate into the chain region via its hydrophobic face, evidence for which is provided by it interacting more readily with all the monolayers tested than LFb does. LFb seems to possess a similar rate of binding with both EH100 or J5 LPS-containing monolayers. However the peptide shows a greater magnitude of change of pressure P_{max} for the Eh-20 monolayer confirming the greater susceptibility of this models compared to J5-20. The LFb peptide layer coverage and thickness (Table 4) on the J5-20 monolayer are higher than on the Eh-20 monolayer hence, for this region, the extent of the pressure change possibly results from a greater concentration at the interfacial region of the model. In fact the percentage of LFb peptide in the inner headgroup of J5-20 is greater than the percentage of LL37 in this same region, hence this may explain the higher change of pressure measured in the monolayer interaction studies. Possibly the more structured J5 LPS-containing monolayer, compared to the EH100, is more resistant to the penetration of LFb and LL37, which accumulate in a thicker peptide layer in proximity to the interface.

The very high concentration of peptide used in the monolayer studies (the lipid:peptide ratio being around 1:2), made necessary by the large aqueous bulk volumes, would promote the interaction of both peptides with the monolayers through electrostatic forces. At such concentrations the subtleties of the possible differential mechanisms of the peptides are not clearly distinct, but it is nevertheless interesting to speculate that the LFb interactions with

the LPS headgroups in the monolayers are favoured because of a concentration-dependent aggregation of the LL37[71] which sequesters it in the adjacent peptide layer observed in the NR experiments. In the ssNMR experiments, where the peptide is at very low concentrations, a differential effect is more noticeable. At the lipid:peptide ratio of 50:1, LL37 has a greater disordering effect on the lipid chains and is therefore more likely to have penetrated into the hydrophobic region of the bilayers than the LFb. The evidence from this study suggests that LFb is less active because it is more likely to localise in the headgroup region of the OM than to penetrate into the bilayer core, and therefore requires a greater concentration in order to induce packing stress and possibly OM perturbation via pore formation.[16,25]

The apparent discrepancies between the results of the NMR and NR studies, serve to highlight some limitations of our model systems, necessitated by our need for stable planar systems for NR. Not the least of these is the fact that the naturally occurring outer membrane contains a limited amount of phosphatidylethanolamines (PE), rather than the phosphatidylcholine incorporated in our systems.[5] The intrinsic curvature of the bacterial OM is not represented in our planar systems since we considered that the requirement for a stable monolayer was more essential. Moreover such curvature effect can be neglected when the bilayer system (OM of a cell or a vesicle) is large and can be comparable to a planar system such as a monolayer.[68] In this regard the models used in this investigation are a compromise in terms of stability and neutrality of the supporting lipid (DPPC), which allowed us to focus solely on the putative charge and steric properties of LPS.

5 Conclusion.

The experiments presented in this study aimed to assess the interactive capacity of LL37 and LFb antimicrobial peptides with models of the outer membrane of Gram negative bacteria composed of DPPC and two different rough chemotypes of LPS. Both the amphiphilic, cationic peptides would be expected to interact with the membrane models by electrostatic attraction to the negative charge of LPS, a by product of which could was the formation

of peptide layers in the vicinity of the interface. The model systems containing the Ra EH100 chemotype of LPS were more susceptible to the activity of LL37 and LFb, than those containing Rc J5, hence a longer core region of the LPS does not seem to provide any greater steric shielding effect in the models we have investigated. Overall our results suggest a deeper penetration of LL37 into the hydrophobic regions of our model systems, whereas LFb localises more in the interfacial region. Biologically this evidence could explain the variable susceptibility of Gram-negative bacteria towards LL37 and LFb, although the naturally occurring OM, with the lipidic component of the outer leaflet comprised mostly of pure LPS,[3,5] might present different physico-chemical properties which affect their activity *in vivo*. It is certain that the interaction of LL37 and LFb peptides is highly dependent upon the structure of the LPSs included in the models determining the binding mechanism of AMPs to the bacterial OM. These results show the benefits of the application of the Gram negative bacteria OM model which includes the presence of lipopolysaccharide; this more closely biomimetic model should increase our knowledge of the mechanism of action of AMPs.

Acknowledgement

This research was financially supported by a Next Generation Facility Users Grant (EPG0685691) from the U.K. Engineering and Physical Sciences Research Council. The authors thank Professor Rob Evans (Brunel University, U.K.) for the generous gift of the peptide bovine Lactoferricin (LFb) used in these experiments. We thank ILL for the allocation of beamtime (experiment reference: http://doi.ill.fr/10.5291/ILL-DATA.8-02-672) and the Partnership for Soft Condensed Matter at ILL Grenoble for the provision of the Langmuir troughs and Brewster angle microscope.

5.1 Supporting Information Available

Supporting Information are provided which include details and results of the solid state Nuclear Magnetic Resonance experiments. Moreover they include additional discussion

concerning the model used in the Neutron Reflectivity experiments.

References

(1) Labischinski, H.; Barnickel, G.; Bradaczek, H.; Naumann, D.; Rietschel, E. T.; Giesbrecht, P. High state of order of isolated bacterial lipopolysaccharide and its possible contribution to the permeation barrier property of the outer membrane. *J. Bacteriol.* **1985**, *162*, 9–20.

(2) Brandenburg, K.; Seydel, U. Investigation into the fluidity of lipopolysaccharide and free lipid A membrane systems by Fourier-transform infrared spectroscopy and differential scanning calorimetry. *Eur. J. Biochem.* **1990**, *191*, 229–236.

(3) Nikaido, H. Prevention of drug access to bacterial targets: permeability barriers and active efflux. *Science* **1994**, *264*, 382–8.

(4) Snyder, D. S.; McIntosh, T. J. The lipopolysaccharide barrier: Correlation of antibiotic susceptibility with antibiotic permeability and fluorescent probe binding kinetics. *Biochemistry* **2000**, *39*, 11777–11787.

(5) Nikaido, H. Molecular Basis of Bacterial Outer Membrane Permeability Revisited. *Microbiol. Mol. Biol. Rev.* **2003**, *67*, 593–656.

(6) Boman, H. G. Antibacterial peptides: basic facts and emerging concepts. *J. Intern. Med.* **2003**, *254*, 197–215.

(7) Boman, H. G. Peptide antibiotics and their role in innate immunity. *Annu. Rev. Immunol.* **1995**, *13*, 61–92.

(8) Nguyen, L. T.; Haney, E. F.; Vogel, H. J. The expanding scope of antimicrobial peptide structures and their modes of action. *Trends Biotechnol.* **2011**, *29*, 464–472.

(9) Fox, J. L. Antimicrobial peptides stage a comeback. *Nat. Biotechnol.* **2013**, *31*, 379–82.

(10) Rietschel, E. T.; Kirikae, T.; Schade, F. U.; Mamat, U.; Schmidt, G.; Loppnow, H.; Ulmer, A. J.; Zähringer, U.; Seydel, U.; Di Padova, F. Bacterial endotoxin: molecular relationships of structure to activity and function. *FASEB J.* **1994**, *8*, 217–25.

(11) Vaara, M. Antibiotic-supersusceptible mutants of Escherichia coli and Salmonella typhimurium. *Antimicrob. Agents Chemother.* **1993**, *37*, 2255–2260.

(12) Yeaman, M. R.; Yount, N. Y. Mechanisms of antimicrobial peptide action and resistance. *Pharmacol. Rev.* **2003**, *55*, 27–55.

(13) Lad, M. D.; Birembaut, F.; Clifton, L. A.; Frazier, R. A.; Webster, J. R. P.; Green, R. J. Antimicrobial peptide-lipid binding interactions and binding selectivity. *Biophys. J.* **2007**, *92*, 3575–86.

(14) Sood, R.; Domanov, Y.; Pietiäinen, M.; Kontinen, V. P.; Kinnunen, P. K. Binding of LL-37 to model biomembranes: Insight into target vs host cell recognition. *Biochim. Biophys. Acta, Biomembr.* **2008**, *1778*, 983–996.

(15) Domenech, O.; Francius, G.; Tulkens, P. M.; Van Bambeke, F.; Dufrêne, Y.; Mingeot-Leclercq, M.-P. Interactions of oritavancin, a new lipoglycopeptide derived from vancomycin, with phospholipid bilayers: Effect on membrane permeability and nanoscale lipid membrane organization. *Biochim. Biophys. Acta* **2009**, *1788*, 1832–40.

(16) Arseneault, M.; Bédard, S.; Boulet-Audet, M.; Pézolet, M. Study of the interaction of lactoferricin B with phospholipid monolayers and bilayers. *Langmuir* **2010**, *26*, 3468–78.

(17) Turner, J.; Cho, Y.; Dinh, N. N.; Waring, A. J.; Lehrer, R. I. Activities of LL-37, a cathelin-associated antimicrobial peptide of human neutrophils. *Antimicrob. Agents Chemother.* **1998**, *42*, 2206–14.

(18) Vandamme, D.; Landuyt, B.; Luyten, W.; Schoofs, L. A comprehensive summary of LL-37, the factotum human cathelicidin peptide. *Cell. Immunol.* **2012**, *280*, 22–35.

(19) Strom, M. B.; Svendsen, J. S.; Rekdal, O. Antibacterial activity of 15-residue lactoferricin derivatives. *J. Pept. Res.* **2000**, *56*, 265–274.

(20) Liu, Y.; Han, F.; Xie, Y.; Wang, Y. Comparative antimicrobial activity and mechanism of action of bovine lactoferricin-derived synthetic peptides. *Biometals* **2011**, *24*, 1069–78.

(21) Théolier, J.; Fliss, I.; Jean, J.; Hammami, R. MilkAMP: a comprehensive database of antimicrobial peptides of dairy origin. *Dairy Sci. Technol.* **2013**, *94*, 181–193.

(22) Bridle, A.; Nosworthy, E.; Polinski, M.; Nowak, B. Evidence of an antimicrobial-immunomodulatory role of Atlantic salmon cathelicidins during infection with Yersinia ruckeri. *PloS one* **2011**, *6*, e23417.

(23) Lars H. Vorland, Hilde Ulvatne, Jill Andersen, Hanne H. Haukland, Øystein Rekdal, John S. Svendsen, T. J. G. Lactoferricin of Bovine Origin is More Active than Lactoferricins of Human, Murine and Caprine Origin. *Scand. J. Infect. Dis.* **1998**, *30*, 513–517.

(24) Aguilera, O.; Ostolaza, H.; Quirós, L.; Fierro, J. Permeabilizing action of an antimicrobial lactoferricin-derived peptide on bacterial and artificial membranes. *FEBS Lett.* **1999**, *462*, 273–277.

(25) Ulvatne, H.; Haukland, H.; Olsvik, O.; Vorland, L. Lactoferricin B causes depolarization of the cytoplasmic membrane of Escherichia coli ATCC 25922 and fusion of negatively charged liposomes. *FEBS Lett.* **2001**, *492*, 62–65.

(26) Nguyen, L. T.; Schibli, D. J.; Vogel, H. J. Structural studies and model membrane interactions of two peptides derived from bovine lactoferricin. *J. Pept. Sci.* **2005**, *11*, 379–89.

(27) Umeyama, M.; Kira, A.; Nishimura, K.; Naito, A. Interactions of bovine lactoferricin with acidic phospholipid bilayers and its antimicrobial activity as studied by solid-state NMR. *Biochim. Biophys. Acta, Biomembr.* **2006**, *1758*, 1523–1528.

(28) Thennarasu, S.; Tan, A.; Penumatchu, R.; Shelburne, C. E.; Heyl, D. L.; Ramamoorthy, A. Antimicrobial and membrane disrupting activities of a peptide derived from the human cathelicidin antimicrobial peptide LL37. *Biophys. J.* **2010**, *98*, 248–57.

(29) Sochacki, K. A.; Barns, K. J.; Bucki, R.; Weisshaar, J. C. Real-time attack on single Escherichia coli cells by the human antimicrobial peptide LL-37. *Proc. Natl. Acad. Sci. U. S. A.* **2011**, *108*, E77–81.

(30) Bello, G.; Eriksson, J.; Terry, A. E.; Edwards, K.; Lawrence, M. J.; Barlow, D. J.; Harvey, R. D. Characterization of the aggregates formed by various bacterial lipopolysaccharides in solution and upon interaction with antimicrobial peptides. *Langmuir* **2014**, *31*, 741–751.

(31) Nagaoka, I.; Hirota, S.; Niyonsaba, F.; Hirata, M.; Adachi, Y.; Tamura, H.; Tanaka, S.; Heumann, D. Augmentation of the lipopolysaccharide-neutralizing activities of human cathelicidin CAP18/LL-37-derived antimicrobial peptides by replacement with hydrophobic and cationic amino acid residues. *Clin. Diagn. Lab. Immunol.* **2002**, *9*, 972–982.

(32) Farnaud, S.; Spiller, C.; Moriarty, L. C.; Patel, A.; Gant, V.; Odell, E. W.; Evans, R. W. Interactions of lactoferricin-derived peptides with LPS and antimicrobial activity. *FEMS Microbiol. Lett.* **2004**, *233*, 193–199.

(33) Chapple, D. S.; Hussain, R.; Joannou, C. L.; Hancock, R. E. W.; Odell, E.; Evans, R. W.; Siligardi, G. Structure and association of human lactoferrin peptides with Escherichia coli lipopolysaccharide. *Antimicrob. Agents Chemother.* **2004**, *48*, 2190–8.

(34) Andrä, J.; Lohner, K.; Blondelle, S. E.; Jerala, R.; Moriyon, I.; Koch, M. H. J.; Garidel, P.; Brandenburg, K. Enhancement of endotoxin neutralization by coupling of a C12-alkyl chain to a lactoferricin-derived peptide. *Biochem. J.l* **2005**, *385*, 135–143.

(35) Clifton, L. A.; Holt, S. A.; Hughes, A. V.; Daulton, E. L.; Arunmanee, W.; Heinrich, F.; Khalid, S.; Jefferies, D.; Charlton, T. R.; Webster, J. R. P.; Kinane, C. J.; Lakey, J. H.

An Accurate In Vitro Model of the E. coli Envelope. *Angew. Chem., Int. Ed. Engl.* **2015**, 11952–55.

(36) Schäfer, H.; Mädler, B.; Sternin, E. Determination of orientational order parameters from 2H NMR spectra of magnetically partially oriented lipid bilayers. *Biophys. J.* **1998**, *74*, 1007–14.

(37) Mason, A. J. et al. Structural determinants of antimicrobial and antiplasmodial activity and selectivity in histidine-rich amphipathic cationic peptides. *J. Biol. Chem.* **2009**, *284*, 119–33.

(38) Inagaki, M.; Kawaura, T.; Wakashima, H.; Kato, M.; Nishikawa, S.; Kashimura, N. Different contributions of the outer and inner R-core residues of lipopolysaccharide to the recognition by spike H and G proteins of bacteriophage phiX174. *FEMS Microbiol. Lett.* **2003**, *226*, 221–7.

(39) Clifton, L. A.; Neylon, C.; Lakey, J. H. Examining protein-lipid complexes using neutron scattering. *Methods Mol. Biol.* **2013**, *974*, 119–50.

(40) Maget-Dana, R. The monolayer technique: a potent tool for studying the interfacial properties of antimicrobial and membrane-lytic peptides and their interactions with lipid membranes. *Biochim. Biophys. Acta, Biomembr.* **1999**, *1462*, 109–140.

(41) Brockman, H. Lipid monolayers: why use half a membrane to characterize protein-membrane interactions? *Curr. Opin. Struct. Biol.* **1999**, *9*, 438–443.

(42) Marsh, D. Lateral pressure in membranes. *Biochim. Biophys. Acta* **1996**, *1286*, 183–223.

(43) Mayer, L.; Hope, M.; Cullis, P.; Janoff, A. Solute distributions and trapping efficiencies observed in freeze-thawed multilamellar vesicles. *Biochim. Biophys. Acta, Biomembr.* **1985**, *817*, 193 – 196.

(44) Leonenko, Z. V.; Finot, E.; Ma, H.; Dahms, T. E. S.; Cramb, D. T. Investigation of temperature-induced phase transitions in DOPC and DPPC phospholipid bilayers using temperature-controlled scanning force microscopy. *Biophys. J.* **2004**, *86*, 3783–93.

(45) Behroozi, F. Theory of elasticity in two dimensions and its application to Langmuir-Blodgett films. *Langmuir* **1996**, *12*, 2289–2291.

(46) Abraham, T.; Schooling, S. R.; Beveridge, T. J.; Katsaras, J. Monolayer film behavior of lipopolysaccharide from pseudomonas aeruginosa at the air-water interface. *Biomacromolecules* **2008**, *9*, 2799–2804.

(47) Risović, D.; Frka, S.; Kozarac, Z. Application of Brewster angle microscopy and fractal analysis in investigations of compressibility of Langmuir monolayers. *J. Chem. Phys.* **2011**, *134*, 024701.

(48) Dynarowicz-Latka, P.; Hac-Wydro, K. Interactions between phosphatidylcholines and cholesterol in monolayers at the air/water interface. *Colloids Surf., B* **2004**, *37*, 21–5.

(49) Rodríguez Patino, J. M.; Sánchez, C. C.; Rodríguez Niño, M. R. Morphological and structural characteristics of monoglyceride monolayers at the airwater interface observed by Brewster angle microscopy. *Langmuir* **1999**, *15*, 2484–2492.

(50) Barlow, D. J.; Hollinshead, C. M.; Harvey, R. D.; Kudsiova, L.; Lawrence, M. J. Memory effects of monolayers and vesicles formed by the non-ionic surfactant, 2C(18)E(12). *J. Colloid Interface Sci.* **2007**, *316*, 741–50.

(51) Campbell, R.; Wacklin, H.; Sutton, I.; Cubitt, R.; Fragneto, G. FIGARO: The new horizontal neutron reflectometer at the ILL. *Eur. Phys. J. Plus* **2011**, *126*.

(52) Hughes, A. RasCAL — SourceForge.net. `http://sourceforge.net/projects/rscl/`.

(53) Burton, M. F.; Steel, P. G. The chemistry and biology of LL-37. *Nat. Prod. Rep.* **2009**, *26*, 1572–1584.

(54) Han, F.-F.; Liu, Y.-F.; Xie, Y.-G.; Gao, Y.-H.; Luan, C.; Wang, Y.-Z. Antimicrobial peptides derived from different animals: comparative studies of antimicrobial properties, cytotoxicity and mechanism of action. *World J. Microbiol. Biotechnol.* **2011**, *27*, 1847–1857.

(55) Henzler-Wildman, K. A.; Martinez, G. V.; Brown, M. F.; Ramamoorthy, A. Perturbation of the hydrophobic core of lipid bilayers by the human antimicrobial peptide LL-37. *Biochemistry* **2004**, *43*, 8459–69.

(56) Lee, Y.-L.; Lin, J.-Y.; Chang, C.-H. Thermodynamic characteristics and Langmuir-Blodgett deposition behavior of mixed (DPPA/DPPC) monolayers at air/liquid interfaces. *J. Colloid Interface Sci.* **2006**, *296*, 647–654.

(57) Ou-Yang, W.; Weis, M.; Yamamoto, T.; Manaka, T.; Iwamoto, M. Effect of external electrostatic charge on condensed phase domains at the air-water interface: Experiment and shape equation analysis. *J. Chem. Phys.* **2009**, *130*, 104706.

(58) Ou-Yang, W.; Weis, M.; Manaka, T.; Iwamoto, M. Study of relaxation process of dipalmitoyl phosphatidylcholine monolayers at air-water interface: effect of electrostatic energy. *J. Chem. Phys.* **2011**, *134*, 154709.

(59) Garcia-Verdugo, I.; Canadas, O.; Taneva, S. G.; Keough, K. M. W.; Casals, C. Surfactant protein A forms extensive lattice-like structures on 1,2-Dipalmitoylphosphatidylcholine/Rough-Lipopolysaccharide- mixed monolayers. *Biophys. J.* **2007**, *93*, 3529–3540.

(60) Canadas, O.; Keough, K. M. W.; Casals, C. Bacterial lipopolysaccharide promotes destabilization of lung surfactant-like films. *Biophys. J.* **2011**, *100*, 108–116.

(61) Mackay, A. L.; Nichol, C. P.; Weeks, G.; Davis, J. H. A proton and deuterium nuclear magnetic reasonance study of orientational order in aqueous dispersions of lipopolysaccharide and lipopolysaccharide/dipalmitoylphosphatidylcholine mixtures. *Biochim. Biophys. Acta, Biomembr.* **1984**, *774*, 181–187.

(62) Kaercher, T.; Hönig, D.; Möbius, D. Brewster angle microscopy. A new method of visualizing the spreading of Meibomian lipids. *Int. Ophthalmol.* **1993**, *17*, 341–8.

(63) Miñones, J.; Rodrguez Patino, J.; Conde, O.; Carrera, C.; Seoane, R. The effect of polar groups on structural characteristics of phospholipid monolayers spread at the airwater interface. *Colloids Surf., A* **2002**, *203*, 273–286.

(64) Chen, X.; Huang, Z.; Hua, W.; Castada, H.; Allen, H. C. Reorganization and caging of DPPC, DPPE, DPPG, and DPPS monolayers caused by dimethylsulfoxide observed using Brewster angle microscopy. *Langmuir* **2010**, *26*, 18902–8.

(65) Le Brun, A. P.; Clifton, L. A.; Halbert, C. E.; Lin, B.; Meron, M.; Holden, P. J.; Lakey, J. H.; Holt, S. A. Structural characterization of a model gram-negative bacterial surface using lipopolysaccharides from rough strains of Escherichia coli. *Biomacromolecules* **2013**, *14*, 2014–22.

(66) Lipp, M. M.; Lee, K. Y.; Waring, A.; Zasadzinski, J. A. Fluorescence, polarized fluorescence, and Brewster angle microscopy of palmitic acid and lung surfactant protein B monolayers. *Biophys. J.* **1997**, *72*, 2783–804.

(67) Krüger, P.; Schalke, M.; Wang, Z.; Notter, R. H.; Dluhy, R. A.; Lösche, M. Effect of hydrophobic surfactant peptides SP-B and SP-C on binary phospholipid monolayers. I. Fluorescence and dark-field microscopy. *Biophys. J.* **1999**, *77*, 903–14.

(68) Feng, S.-S. Interpretation of mechanochemical properties of lipid bilayer vesicles from the equation of state or pressure area measurement of the monolayer at the airwater or oilwater interface. *Langmuir* **1999**, *15*, 998–1010.

(69) Vaknin, D.; Kjaer, K.; Als-Nielsen, J.; Lösche, M. Structural properties of phosphatidylcholine in a monolayer at the air/water interface: Neutron reflection study and reexamination of x-ray reflection measurements. *Biophys. J.* **1991**, *59*, 1325–32.

(70) Clifton, L. A.; Skoda, M. W. A.; Daulton, E. L.; Hughes, A. V.; Le Brun, A. P.; Lakey, J. H.; Holt, S. A. Asymmetric phospholipid: lipopolysaccharide bilayers; a Gram-negative bacterial outer membrane mimic. *J. R. Soc., Interface* **2013**, *10*, 20130810.

(71) Hwang, P. M.; Zhou, N.; Shan, X.; Arrowsmith, C. H.; Vogel, H. J. Three-dimensional solution structure of lactoferricin B, an antimicrobial peptide derived from bovine lactoferrin. *Biochemistry* **1998**, *37*, 4288–4298.

(72) Brandenburg, K.; Funari, S.; Koch, M.; Seydel, U. Investigation into the Acyl Chain Packing of Endotoxins and Phospholipids under Near Physiological Conditions by WAXS and FTIR Spectroscopy. *J. Struct. Biol.* **1999**, *128*, 175–186.

(73) Wu, E. L.; Engström, O.; Jo, S.; Stuhlsatz, D.; Yeom, M. S.; Klauda, J. B.; Widmalm, G.; Im, W. Molecular dynamics and NMR spectroscopy studies of E. coli lipopolysaccharide structure and dynamics. *Biophys. J.* **2013**, *105*, 1444–1455.

TOC Graphic

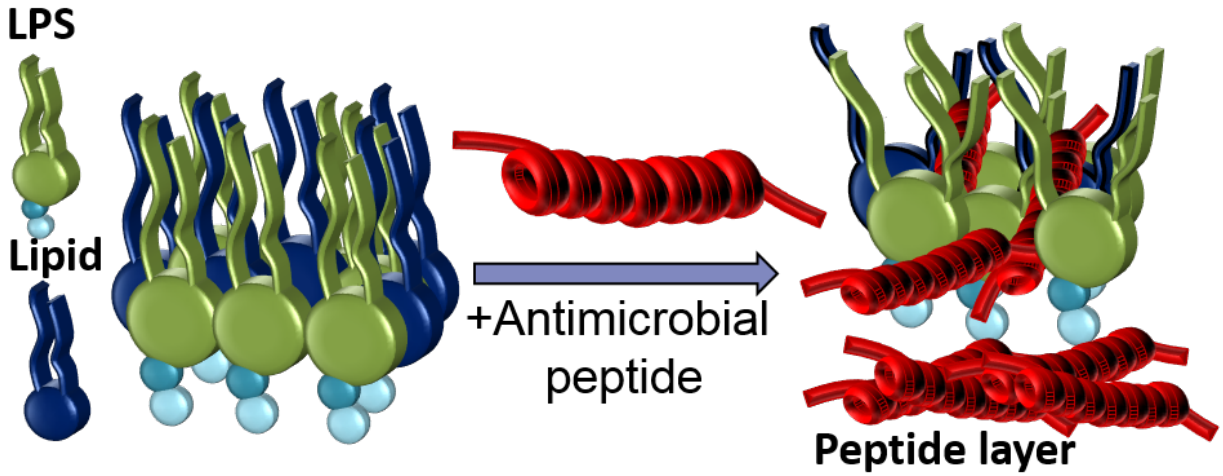

Figure 8: Table of Contents Graphic file *float/TOCgraphic.tif*